



**HAL**  
open science

# Oxidation behaviour at 1100°C in air of 25 wt-% Cr-containing cobalt-based alloys containing high quantities of hafnium carbides

Patrice Berthod, Elodie Conrath

► **To cite this version:**

Patrice Berthod, Elodie Conrath. Oxidation behaviour at 1100°C in air of 25 wt-% Cr-containing cobalt-based alloys containing high quantities of hafnium carbides. *Canadian Metallurgical Quarterly*, 2016, 55 (4), pp.409-419. 10.1080/00084433.2016.1206290 . hal-02510127

**HAL Id: hal-02510127**

**<https://hal.science/hal-02510127>**

Submitted on 17 Mar 2020

**HAL** is a multi-disciplinary open access archive for the deposit and dissemination of scientific research documents, whether they are published or not. The documents may come from teaching and research institutions in France or abroad, or from public or private research centers.

L'archive ouverte pluridisciplinaire **HAL**, est destinée au dépôt et à la diffusion de documents scientifiques de niveau recherche, publiés ou non, émanant des établissements d'enseignement et de recherche français ou étrangers, des laboratoires publics ou privés.

# Oxidation behavior at 1100°C in air of 25wt.%Cr-containing cobalt-based alloys containing high quantities of hafnium carbides

Patrice Berthod\* and Elodie Conrath

Institut Jean Lamour (UMR CNRS 7198)  
Department Chemistry and Physics of Solids and Surfaces  
Team "Surface and Interfaces, chemical reactivity of materials"  
Faculty of Sciences and Technologies, Boulevard des Aiguillettes, B.P. 70239, 54506  
Vandoeuvre-lès-Nancy, France

\*Corresponding author:

Phone: (+33)383684666, Fax; (+33)383684611,

E-mail: [patrice.berthod@univ-lorraine.fr](mailto:patrice.berthod@univ-lorraine.fr)

Postprint version of the article:

**Canadian Metallurgical Quarterly 2016 VOL 55 N° 4 409-419.**

*DOI: 10.1080/00084433.2016.1206290*

## Abstract:

Hafnium, usually added to improve the high temperature oxidation resistance of alloys, allowed obtaining HfC carbides which are very efficient for the creep-resistance. For that Hf must be added in particularly high quantities which may possibly influence the oxidation behavior. Three HfC-strengthened cast cobalt alloys were studied all along thermogravimetry tests at 1100°C. They were compared to similar but Hf-free ternary alloys. The mass variation were plotted according to  $\{m \times dm/dt = f(-m)\}$  to specify all kinetic oxidation constants, and versus temperature to study the oxidation beginning during heating and the scale spallation during cooling. The presence of many HfC carbides obviously influences the high temperature oxidation: mass gain occurring sooner during heating, faster isothermal mass gains but better behavior in oxide scale spallation during cooling. This deterioration of oxidation behavior must be corrected to hope benefiting from the high creep-resistance brought by this new type of strengthening.

**Keywords:** Cobalt-based alloys; Hafnium carbides; Isothermal oxidation; Oxidation at heating; Oxide spallation at cooling; Oxide characterization

## Introduction:

Many high temperature applications require geometrically complicated metallic pieces and the classical foundry way is often essential to allow complex-shaping<sup>1</sup> as well as coarse-grained microstructures to keep high creep-resistance. The obtained polycrystalline alloys present multiple randomly oriented grain boundaries which are the mechanically weakest zones in the microstructures. When the alloys must be used under stresses at temperatures higher than the equi-cohesive temperature, their grain boundaries must be reinforced by hard particles. These ones can be the eutectic carbides which appeared at the end of solidification in the interdendritic spaces. This is the case of the acicular chromium carbides or script-like tantalum carbides which are often exploited in carbon-containing cast cobalt-based superalloys<sup>2</sup>. The carbides mechanically strengthening grain boundaries must be very stable at the high temperatures of work. Chromium carbides do not meet this requirement since their volume fractions rapidly decrease at high temperature. More stable, the tantalum carbides are nevertheless sometimes not heat-resisting enough since they get fragmented too rapidly<sup>3</sup> with as result significant loss in high temperature mechanical resistance<sup>4-6</sup>. Other MC carbides (i.e. monocarbide of a "M" metal, "M" being Ta for example) are particularly resistant to morphological changes at high temperature: the HfC carbides recently obtained in solidified cobalt-based alloys<sup>7</sup> with a script-like shape and forming an interdendritic eutectic compound with matrix.

For several decades hafnium was mainly considered as an element beneficial for the high temperature oxidation behavior of superalloys. Its actions in this field are slowing the oxide growth or improving the protective oxides adherence<sup>8</sup>. According to recent articles, the used Hf contents were generally close to 1 wt.% (typically between 0.25 and 1.5 wt.%) in commercial alloys<sup>10</sup>, iron- based bulk alloys rich in Cr and Al<sup>11</sup>, aluminides<sup>12</sup> and TBC-supporting bond coats<sup>13</sup>. Hafnium was recently used in alloys for use at high temperature in order to develop a particularly efficient strengthening interdendritic network of HfC carbides. Their mechanical properties at temperatures up to 1200°C were remarkable for cast polycrystalline alloys simply reinforced by carbides<sup>14</sup>. However, alloys containing so high Hf contents, an element which is particularly easy to oxidize at high temperature, may present particular behaviors in oxidation at high temperature, which may be interesting to explore. This is what was

undertaken in the present study for 1100°C, temperature at which the best actual superalloys - the  $\gamma/\gamma'$  Ni-based single-crystals - lose their principal strengthening particles, with three cast Co-based alloys containing various volume fractions in HfC carbides. In parallel two cobalt-based ternary alloys with the same contents in chromium and carbon but without hafnium were also studied in order to specify the base behavior and then, by comparison, the influence of the hafnium carbides.

## Experimental methods

### *Alloys' elaboration*

For each alloy a total charge of about 40 grams of pure elements (>99.9 wt.%, Alfa Aesar) was prepared, according to the following compositions (in weight percents):

- “CoHf1” alloy: Co(bal.)-25Cr-0.25C-3.7Hf (atomic equality between C and Hf)
- “CoHf2a” alloy: Co(bal.)-25Cr-0.5C-3.7Hf (C atomic content equal to twice the Hf one)
- “CoHf2b” alloy: Co(bal.)-25Cr-0.5C-7.4Hf (atomic equality between C and Hf again, double HfC population expected by comparison with the CoHf1 alloy)
- “Co1” alloy: Co-(bal.)-25Cr-0.25C (to which the CoHfC1 alloy will be compared)
- “Co-2”: Co(bal.)-25Cr-0.50C (to which the CoHf2a and CoHf2b alloys will be compared).

The elaboration of these alloys, whose compositions are summarized in Table 1, was carried out using a High Frequency induction furnace (CELES, France; operating parameters: voltage 4kV and frequency 110kHz). Melting, the 3 minutes-dwell and solidification of the alloys took place in a water-cooled copper crucible present in the fusion chamber of the furnace, in a surrounding inert gaseous environment (300 mbars of pure argon). Compact ingots were obtained, and after complete cooling, they were cut to obtain the parts needed for the characterization of the as-cast microstructures of the alloys as well as the one destined to the high temperature oxidation tests.

### *Thermogravimetry tests and kinetic exploitations*

The parts destined to the high temperature oxidation tests were cut to obtain parallelepipeds of about  $8 \times 8 \times 3 \text{ mm}^3$ . These ones were ground, first by using 240-grit SiC papers to smooth edges and corners, and second all around with 1200-grit SiC papers.

A sample of each of the five alloys was subjected to high temperature oxidation in a thermo-balance. The used apparatus was a SETARAM TGA92 one. Tests were done in a constant flow of synthetic air (80%  $\text{N}_2$  – 20%  $\text{O}_2$ ). In each case, after a heating at  $+20 \text{ }^\circ\text{C min}^{-1}$ , the samples were maintained at  $1100^\circ\text{C}$  during 50 hours, then cooled at  $-5 \text{ }^\circ\text{C min}^{-1}$ , rate expected low enough to limit the spallation of the oxide scale developed all over the sample.

The mass gain files (record step: about 40s) were thereafter exploited with a spreadsheet program. It was first verified, by plotting versus time the mass gain recorded during the  $1100^\circ\text{C}$ -stage, that the isothermal oxidation kinetic was globally parabolic type and then that it seemingly follows the Wagner's law. This parabolic regime may be preceded by an initial short linear transient oxidation, the linear constant of which,  $K_l$ , was determined. The isothermal part of the mass gain files was first classically treated to determine the parabolic constant  $K_p$ , by plotting mass gain versus the square root of time and by noting the average slope of the obtained more or less straight curve.

Since the studied alloys possibly present a chromia-forming behavior thanks to the 25wt.%Cr that they contain, a minimization of the oxidation rate when assessed from mass gain results may occur because of the possible mass loss by chromia volatilization. This phenomenon, re-oxidation of  $\text{Cr}_2\text{O}_3$  in volatile  $\text{CrO}_3$  is expected in air when temperature is higher than  $1000^\circ\text{C}$ . Even at  $1100^\circ\text{C}$  chromia volatilization must be taken into account, by determining the chromia volatilization constant  $K_v$  together with  $K_p$ . For this purpose one used a method recently developed<sup>15</sup>. This one consists in plotting, versus  $\{-m\}$  (opposite of the mass gain per surface unit area), the product  $\{m \times dm/dt\}$  (the mass gain per surface unit area multiplied by the same quantity but derived by regard to time). After a first transient part, the  $\{m \times dm/dt\}$  plotted versus  $\{-m\}$  becomes a straight line obeying the  $\{m \times dm/dt = K_p - m \times K_v\}$  equation. The parabolic constant  $K_p$  and the chromia volatilization constant  $K_v$  can be

thus easily deduced as, respectively, the ordinate at the origin and the slope of the straight line.

Before that, the mass gain during the heating (performed in presence of synthetic air) was specified. This first mass gain needs to be known and added to the eventual linear mass gain to allow an accurate determination of  $K_p$  (or  $K_p-K_v$ ) since the oxide thickness already existing at the beginning of the isothermal stage influences the parabolic regime. Since the used thermo-balance was not a symmetric one, the mass gain at heating and the one at cooling were corrected from the air buoyancy variations as done in an earlier work<sup>16</sup>. For this the mass gains were plotted versus temperature instead of time, and corrected from the apparent mass variations due to the buoyancy variations of the heated air. The corrected curves of mass gain versus temperature during the heating allow specifying first the temperature at which the mass gain really due to oxidation becomes to be detectable by the used thermo-balance. This criterion is of course not absolute since it closely depends on the used thermo-balance. However the comparison of these “oxidation start” temperatures between the different alloys oxidized in the same thermo-balance and for the same oxidizing atmosphere and heating rate, may be very interesting.

The cooling parts of these curves of mass gain, corrected from the air buoyancy variations and plotted versus temperature, can give indications about oxide spallation<sup>17</sup>. The deduced parameters were the temperatures at which oxide spallation started and the final mass variation during the whole cycle.

### *Metallography characterization*

The parts destined to the observations of the as-cast microstructures were embedded in a cold mixture composed of a liquid resin (DBF from ESCIL, 82% in mass) and a hardener (HY956 from ESCIL, 18%). They were thereafter ground, using first SiC papers with grades from 120 or 240 up to 1200 under water, and second, after intermediate ultra-sonic cleaning, polished using a textile disk enriched with diamond particles (ESCIL) to obtain a mirror-like surface state.

After the oxidation tests the samples were first subjected to X-ray diffraction analysis (Philips X'Pert Pro MPD diffractometer, copper anode, wavelength  $\lambda=1.5406$

Ångströms) to identify the oxides formed on surface. Second they were coated with a fine gold layer to give electric conductivity to their surface (despite the presence of external oxide scales). This was done to allow thereafter an electrolytic deposition of a thick nickel shell destined to protect the oxide scales from loss during cutting. The gold-covered oxidized samples were immersed in a warm (50°C) Watts' bath (aqueous solution of Ni<sup>2+</sup> ions prepared from mainly NiSO<sub>4</sub> and NiCl<sub>2</sub> salts) to allow the deposition of metallic nickel by reduction of the Ni<sup>2+</sup> cations under a current density of about 1.6 A/dm<sup>2</sup>. After cutting the oxidized samples in two parts, cross-sections were prepared by following the same metallographic preparation details (embedding-grinding-polishing) as for the samples for the as-cast microstructure examinations.

The global chemical composition of each as-cast alloy was controlled using the Energy Dispersive Spectrometry (EDS) device attached to a Scanning Electron Microscope (SEM, model: JSM6010LA from JEOL), under an acceleration voltage of 20kV

The initial microstructures of the as-cast alloys were examined using the SEM, mainly in the Back Scattered Electrons mode (BSE). The oxide scales and the subsurface microstructures (in cross section) were also examined by SEM/BSE and analyzed by spot SEM/EDS measurements. Additionally, successive spot EDS analyses were performed in the alloy at an increasing depth from the oxide/alloy interface, perpendicularly to later one. This aimed to specify the concentration profiles in Cr and Hf in the subsurface, in order to better describe the deterioration of the external part of the alloys due to oxidation.

## **Results and discussion**

### *As-cast microstructures of the alloys*

The microstructures of the three Hf-rich alloys in their as-cast conditions are illustrated in Fig. 1 (SEM images taken in BSE mode). They present an interdendritic network of script-like HfC carbides. These ones are in the CoHf2a alloy as numerous as in the CoHf1 one, while they are much more present in the CoHf2b alloy. In addition to the interdendritic script-like HfC carbides one can note the presence of

other HfC carbides, geometrically different. These ones, more compact, have precipitated at the beginning solidification: they are pro-eutectic HfC carbides while the script-like HfC ones have precipitated as eutectic with matrix. The volume fraction of HfC carbides of both types is obviously closely dependent on the Hf content in the alloy, and not on the carbon content. Dark particles are additionally present in the CoHf2a alloy. They are chromium carbides. The two ternary alloys are composed of matrix and of chromium carbides. These carbides are however rather rare in the Co1 alloy. In contrast they are more present in the Co2 one (higher carbon content), in the interdendritic spaces. For a given carbon content the presence of hafnium obviously leads to much more carbides than in the ternary alloys. This shows that Hf is a much stronger carbides-forming element. Some pinpoint EDS measurements performed in the matrix showed that hafnium is totally absent in the matrix of the Hf-rich alloys. This indicates that all the hafnium atoms have formed HfC.

#### *Isothermal oxidation*

The mass gain curves plotted versus time are all displayed in Fig. 2. The two 0.25C-containing alloys (Fig. 2 top) led to no really parabolic curves. Indeed, the mass gain of the Hf-rich one was a long time almost linear before becoming more parabolic, and the Hf-free one was linear during a short time, thereafter parabolic for about 30 hours until mass gain accelerated again. The three 0.50C-containing alloys (Fig. 2 bottom) led to much more parabolic curves than the two previous ones. The oxidation rates seem to be higher in presence of hafnium, and the higher the Hf content the faster the mass gain rate. This is confirmed by the results of kinetic exploitation of the mass gain files (Table 2):

- $K_l$  constants: rather scattered results ( $8$  to  $40 \times 10^{-8} \text{ g cm}^{-2} \text{ s}^{-1}$ ), no evident dependence on the carbon and hafnium contents
- $K_p$  constants (classically determined): parabolic kinetics faster in presence of Hf (from about  $80$  to about  $270 \times 10^{-12} \text{ g}^2 \text{ cm}^{-4} \text{ s}^{-1}$ , against about  $15 \times 10^{-12} \text{ g}^2 \text{ cm}^{-4} \text{ s}^{-1}$  for the two Hf-free alloys); higher  $K_p$  values noticed in presence of only HfC (CoHf1 and CoHf2b), lower values in presence of chromium carbides (Co1, Co2 and even CoHf2a which contains a little chromium carbides in addition to HfC)

- $K_v$  constants: significantly higher for the Hf-rich alloys (from about 270 to about  $400 \times 10^{-10} \text{ g cm}^{-2} \text{ s}^{-1}$ , against 40 to  $80 \times 10^{-10} \text{ g cm}^{-2} \text{ s}^{-1}$  for Co1 and Co2); this does not change the  $K_p$  hierarchy between the Hf-free alloys (from about 20 to about  $40 \times 10^{-12} \text{ g}^2 \text{ cm}^{-4} \text{ s}^{-1}$ ) and the Hf-rich ones (from about 240 to about  $470 \times 10^{-12} \text{ g}^2 \text{ cm}^{-4} \text{ s}^{-1}$ ).

The values of kinetic constants  $K_p$  and  $K_v$ , particularly high for the Hf-rich alloys, were however accurately determined and validated by comparison between experimental curve and mathematical ones plotted from the determined values of  $K_p$  and  $K_v$ . The  $\{m \times dm/dt = f(-m) = K_p - m \times K_v\}$  method well led to really straight lines the equation of which allowed determining the two constants (e.g. Fig. 3), which were validated by a very faithful mathematical curve (green dotted line in Fig. 4, much closer to the thick grey experimental curve than the thin red mathematical curve plotted with the  $K_p$  value classically determined).

#### *Oxidation at heating and scale spallation at cooling*

The mass gains during heating are plotted versus temperature in Fig. 5 (top) for the 0.25C-containing alloys and in Fig. 5 (bottom) for the 0.50C-containing ones. One can see that the mass gain by oxidation became detectable by the thermo-balance sooner for a lower carbon content (i.e. at lower temperature) than for a higher one, and for a Hf-rich alloy than for a Hf-free one. These observations, confirmed in Table 3 by the values of oxidation start temperature, let think first that a more dense interdendritic carbide network tends favoring an early oxidation during heating by exposing more the highly oxidable elements (Cr, Hf) to hot air, and second a more oxidable carbide-former element leads to the same effect by a better reactivity with oxygen. In contrast, the total mass gain achieved during the whole heating does not follow a clear law versus the carbon and hafnium contents (Table 3).

Plotting mass gain or variation versus temperature allows evidencing the moment at which the oxide scales, previously formed during heating and mainly during the isothermal stage, started to be lost (Fig. 6). These curves, as well as the values resulting of their exploitation and which are displayed in Table 4, show that the spallation of the external oxide scales occurred in all cases, but it started after a

cooling down to a temperature which was significantly lower for the alloys containing hafnium than for the Hf-free ternary ones. As a result the total mass change is positive for the Hf-containing alloys and negative for the ternary ones. Thus, besides its principal role of carbides stabilizer at high temperature and consequently of high temperature mechanical properties upholder, hafnium remained efficient as scale adherence favoring element, despite its particularly high contents here.

#### *Pre-cutting oxide scale characterization*

The surfaces of the oxidized samples are illustrated in Fig. 7 by macrographs taken using a simple office scanner. They confirm that the scales formed on all alloys tended to spall off during cooling but also that final spallation state was more severe for the Hf-free alloys than for the Hf-rich ones. XRD measurements were carried out on the oxidized surfaces of the samples before they were cut. Results (Table 5) showed that chromia ( $\text{Cr}_2\text{O}_3$ ) was present at the surface of all alloys, but it was never the single oxide present. The  $\text{CoCr}_2\text{O}_4$  spinel oxide, and even the simple CoO cobalt oxide were often present too. The  $\text{HfO}_2$  oxide was also detected on the oxidized surfaces of the three Hf-rich alloys.

#### *Cross-sectional characterization of oxide scales and subsurface deterioration*

The thickness of the scales as well as the amounts and locations of the different oxides revealed by XRD necessitated cross-section preparations. Per alloy two cross-sectional SEM/BSE micrographs taken at two magnifications (left: general view, and right: detailed view) are presented in Fig. 8 for the two 0.25C-containing alloys and in Fig. 9 for the three 0.50C-containing alloys. First, one can globally see that the total thickness of the external scales (including all types of oxides) tends to be higher for the Hf-rich alloys than for the Hf-free ones. This is in good agreement with the mass gain hierarchies. Second, instead of being the main oxide existing in the scales, chromia is less present than CoO and than the spinel oxide. Chromia is generally situated in the most inner position, inside the alloy where it constitutes a more or less continuous and geometrically complex internal layer. Just above one meets the spinel oxide and after, the most external one, the cobalt oxide CoO. It seems that the external cobalt oxide CoO layer has grown outward by cationic

diffusion of  $\text{Co}^{2+}$  while the medium spinel oxide  $\text{CoCr}_2\text{O}_4$  and the internal chromia  $\text{Cr}_2\text{O}_3$  both have grown inward by anionic diffusion of  $\text{O}^{2-}$ . This scheme seems validated by the position of the hafnium oxides  $\text{HfO}_2$  which resulted from the *in situ* oxidation of the HfC carbides: they are disseminated inside chromia and the spinel oxide but never in the outer cobalt oxide scale. The oxidized HfC carbides seem playing the role of the gold marks that one sometimes deposits on slightly pre-oxidized alloys in order to reveal the cationic or anionic character of diffusion during the subsequent high temperature oxidation. One can underline that, concerning the observed diffusion phenomena, the studied alloys did not differ from what is commonly known about more common cobalt-based alloys<sup>8</sup> and notably ternary Co-Cr-C and ternary Co-Cr alloys. The presence of hafnium did not influence the diffusion phenomena usually observed for the existing cobalt-based alloys, which is not surprising since Hf is exclusively present as HfC carbides (no Hf atoms in solid solution in the matrix), carbides which are *in situ* transformed into isolated internal  $\text{HfO}_2$  oxides without any diffusion of the Hf atoms.

The alloys' chemical compositions in outermost surface were specified by EDS spot analysis, five times per oxidized alloys. The results, presented in Table 6, reveal that the chromium contents have become rather low: around 13 wt.% for three of the alloys, and even 8wt.% for the CoHf1 alloy. These values are not compatible with the sustainability of any chromia-forming behavior, which was effectively lost as demonstrated by the analyses of the present oxides (major part is composed of cobalt oxide and of spinel oxide). The Co1, Co2 and CoHf2a alloys (13-14 wt.%Cr in outermost surface) present a rather regular/linear scale/alloy interface. In contrast oxidation has clearly become catastrophic for the CoHf1 and CoHf2b alloy (mass gain of about 0.01g/cm<sup>2</sup> after 50 hours at 1100°C). This resulted in a chromium content of only 8wt.%Cr in outermost surface (very low) for the first alloy, and in a Cr content of almost 18wt.% for the second one, a particularly high value which shows that the alloy started to be consumed by the inward progression of the catastrophic oxidation. Concerning Hf it is almost absent in the outermost surface as in the matrix elsewhere. Obviously the HfC carbides close to the scale/alloy interface are transformed in oxides *in situ* without any release of Hf atoms. Indeed the EDS profiles given in Fig. 10 show that the Hf content is often zero and jumps at high level when HfC carbides are touched by the electron beam of the SEM. On these profiles one can see that the chromium content regularly but rapidly decreases from a 50 to

80  $\mu\text{m}$  depth in the bulk when one goes to the scale/alloy interface where it reaches very low levels. In the case of the CoHf2b alloy for which catastrophic oxidation penetrated the alloy the Cr content at the oxidation front is maintained at a rather high level because of the oxidation of all the elements belonging to the alloy.

## Conclusions

Hafnium carbides present important advantages for strengthening cast superalloys: their script-like morphology, their imbrication with matrix in an eutectic compound, their very high stability at high temperature, notably. This, associated with an intrinsically mechanically resistant cobalt-based matrix, recently proved that they allowed high mechanical properties at levels of working temperature considered forbidden for polycrystalline cast alloys. However, it was here demonstrated that the same combination of a cobalt matrix reputed to be less resistant against high temperature oxidation than corresponding nickel alloys (essentially for Cr diffusion easiness reasons), with HfC carbides made from a particularly oxidable element, does not allow oxidation resistance high enough to envisage industrialization and use in the present state. Further work needs to be carried out. The improvement of these alloys in oxidation behavior requires additional work and changes in the chemical composition, for example by enriching them in chromium beyond the actual 25 wt.% (30 wt.% or more) or by addition of aluminum and/or silicon. Cr deposition by pack-cementation or by other Chemical Vapor Deposition techniques can be also considered. In another side, the high easiness of hafnium oxidation is probably not the single reason of the deterioration of the oxidation resistance of the base alloys Co-25Cr-0.25 and 0.50C. The cross-sectional observations clearly showed that the HfC carbides initially present close to the oxide/alloy interface did not disappear unlike chromium carbides or tantalum carbides for example. They are transformed into  $\text{HfO}_2$  oxides which stay on place even close to the oxidation front and then obstruct chromium diffusion along the grain/interdendritic boundaries. This is possible that they permanently disturb the supply of the oxidation front in chromium and thus favor a precocious generalized oxidation by loss of the chromia-forming behavior: outward cationic  $\text{Cr}^{3+}$  diffusion shortly replaced by inward anionic  $\text{O}^{2-}$  diffusion. The

effect of HfC on the different phenomena governing the oxidation process remains to be analyzed and clearly explained.

### **Acknowledgements:**

The authors would like thank Pascal Villeger for the XRD experiments.

### **References:**

1. C. T. Sims and W. C. Hagel (eds.): 'The Superalloys'; 1972, New York, John Wiley & Sons.
2. C.T. Sims, N.S. Stoloff and W.C. Hagel (eds): 'Superalloy II – High temperature materials for aerospace and industrial power'; 1987, New York, John Wiley.
3. P. Berthod, S. Michon, L. Aranda, S. Mathieu and J.C. Gachon: 'Experimental and thermodynamic study of the microstructure evolution in cobalt-base superalloys at high temperature', *Calphad*, 2003, **27**, 353-359.
4. M. J. Donachie and S. J. Donachie (eds): 'Superalloys – A technical guide (2<sup>nd</sup> ed.)'; 2002, Materials Park, ASM International.
5. P. Berthod, S. Michon, L. Aranda and P. Steinmetz: 'Consequences of the high temperature microstructure evolution on the tensile properties at high temperature of a cobalt-based superalloys reinforced by tantalum carbides', Proc. 'Matériaux 2006', Dijon, France, November 2006.
6. P. Berthod, C. Heil and L. Aranda: 'Influence of the morphologic evolution of the eutectic carbides at high temperature on the thermal expansion behaviour of refractory cast alloys', *J. Alloys Compd*, 2010, **504**, 243-250.
7. P. Berthod: 'High temperature properties of several chromium-containing Co-based alloys reinforced by different types of MC carbides (M=Ta, Nb, Hf and/or Zr)', *J. Alloys Compd*, 2009, **481**, 746-754.
8. D. J. Young: 'High temperature oxidation and corrosion of metals'; 2008, Amsterdam, Elsevier.

10. W. S. Lee and G. M. Kim: 'The effect of Hf, Y and Zr additions on the oxidation behaviour of Ni-based Inconel 601 at high temperature', *Han'guk Pusik Hakhoechi*, 1995, **24**, 124-133.
11. K. Ishii, M. Kohno, S. Ishikawa and S. Satoh: 'Effect of Ti, Zr and Hf on high-temperature oxidation resistance of Fe-20Cr-5Al-0.1La alloy foils', *Materials Transactions JIM*, 1998, **39**, 1040-1045.
12. X. Chunmei, J. Guo and F. Yang: 'High-temperature oxidation behaviour of NiAl-28Cr-5Mo-1Hf alloy', *Jinshu Xuebao*, 2001, **37**, 857-860.
13. H. Guo, L. Sun, H. Li and S. Gong: 'High temperature oxidation behaviour of hafnium modified NiAl bond coat in EB-PVD thermal barrier coating system', 2008, *Thin Solid Films*, **516**, 5732-5735.
14. P. Berthod and E. Conrath: 'Mechanical and Chemical Properties at High Temperature of {M-25Cr}-based Alloys Containing Hafnium Carbides (M=Co, Ni or Fe): Creep Behavior and Oxidation at 1200°C', *J. Mater. Sci. Technol. Res.*, 2014, **1(1)**, 7-14.
15. P. Berthod: 'Kinetics of high temperature oxidation and chromia volatilization for a binary Ni-Cr alloy', *Oxid. Met.*, 2005, **64**, 235-252.
16. P. Berthod: 'Oxidation start detection on heating parts of thermogravimetry curves for high temperature alloys based on nickel, cobalt or iron', *Open Corr. J.*, 2011, **4**, 1-8.
17. P. Berthod: 'Thermogravimetric study of oxide spallation for chromium-rich cast cobalt-based and iron based alloys oxidized at high temperature', *Open Corr. J.*, 2009, **2**, 61-70.

## TABLES

Table 1. Chemical compositions of the five studied alloys (all contents in weight percents)

elements	Cr	C (expected)	Hf
Co1	25	0.25	/
CoHf1	25	0.25	3.7
Co2	25	0.50	/
CoHf2a	25	0.50	3.7
CoHf2b	25	0.50	7.4

Table 2. Values of the kinetic constants determined from the mass gain files

Constants	$K_i$	$K_p$		$K_v$
	( $\times 10^{-8} \text{ g cm}^{-2} \text{ s}^{-1}$ )	( $\times 10^{-12} \text{ g}^2 \text{ cm}^{-4} \text{ s}^{-1}$ )		( $\times 10^{-10} \text{ g cm}^{-2} \text{ s}^{-1}$ )
alloys	slope at stage start	classic	$m \times dm/dt = f(-m)$	$m \times dm/dt = f(-m)$
Co1	7.73	12.4	19.4	40.1
CoHf1	19.5	253	433	267
Co2	39.2	15.4	41.4	80.8
CoHf2a	15.7	76.0	242	395
CoHf2b	29.6	274	470	268

Table 3. Oxidation behavior during heating: temperature of oxidation start (according to the accuracy of the used thermobalance) and total mass gain achieved by oxidation before the isothermal stage beginning

Alloys	Temperature of oxidation start ( $^{\circ}\text{C}$ )	Mass gain during heating ( $\text{mg cm}^{-2}$ )
Co1	844	0.056
CoHf1	819	0.089
Co2	932	0.098
CoHf2a	847	0.069
CoHf2b	859	0.136

Table 4. Oxidation behavior during cooling: temperature of scale spallation start and final mass variation after the whole thermal cycle

Alloys	Temperature of spallation start ( $^{\circ}\text{C}$ )	Final mass variation ( $\text{g cm}^{-2}$ )
Co1	578	-0.004
CoHf1	385	+0.003
Co2	460	-0.003
CoHf2a	416	0.000
CoHf2b	340	+0.006

Table 5. Natures of the various oxides present in the external scales (XRD results)

Alloys	Composition of the oxide scales
Co1	CoO – CoCr <sub>2</sub> O <sub>4</sub> – Cr <sub>2</sub> O <sub>3</sub>
CoHf1	CoO – CoCr <sub>2</sub> O <sub>4</sub> – Cr <sub>2</sub> O <sub>3</sub>
Co2	CoO – Cr <sub>2</sub> O <sub>3</sub>
CoHf2a	CoCr <sub>2</sub> O <sub>4</sub> – Cr <sub>2</sub> O <sub>3</sub> – HfO <sub>2</sub>
CoHf2b	CoO – CoCr <sub>2</sub> O <sub>4</sub> – Cr <sub>2</sub> O <sub>3</sub> – HfO <sub>2</sub>

Table 6. Contents in chromium and in hafnium in outermost surface (average, standard deviation and range determined from values obtained in five randomly chosen locations); EDS spot analysis

Elements in outermost surface	Average wt.%Cr	Std deviation wt.%Cr	wt.% Hf range
Co1	13.1	4.1	/
CoHf1	8.2	2.2	0.0
Co2	13.9	1.7	/
CoHf2a	13.0	0.5	0.0
CoHf2b	17.6	1.2	0 - 0.04

# FIGURES

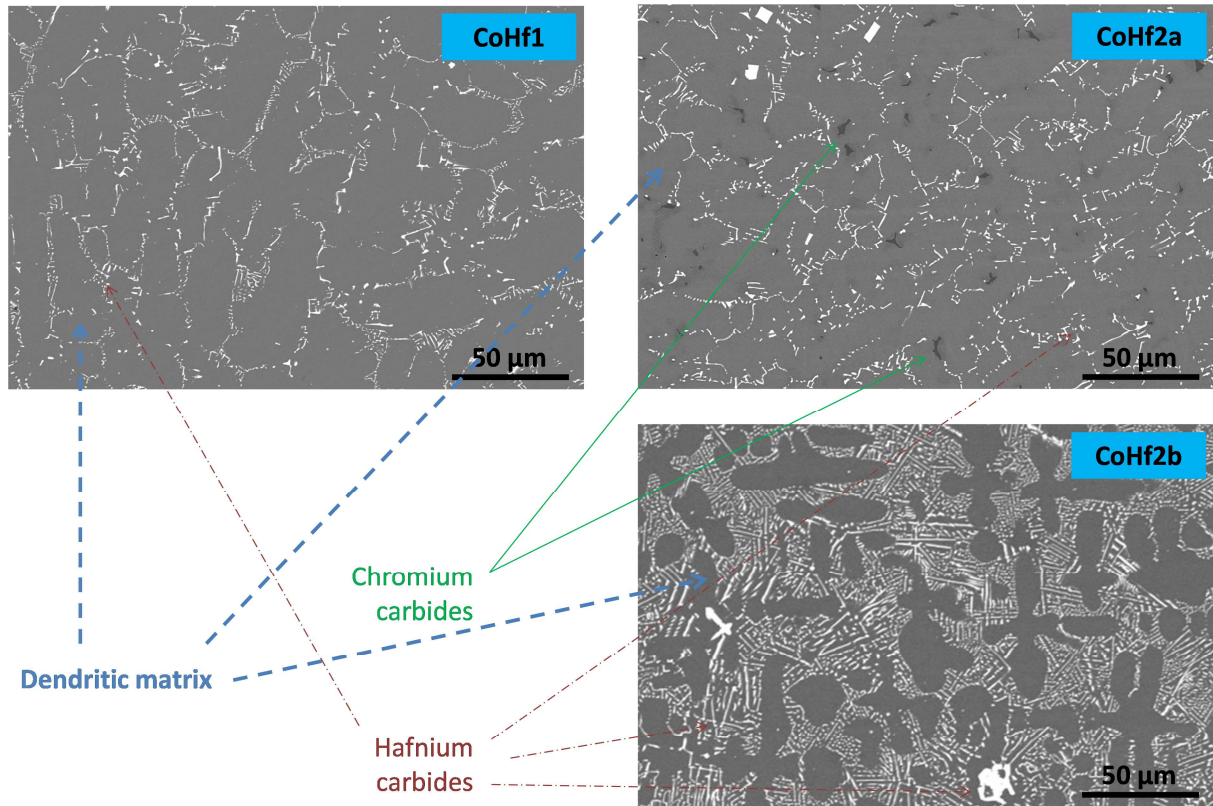


Fig. 1. As-cast microstructures of the three Hf-rich alloys (SEM/BSE examinations)

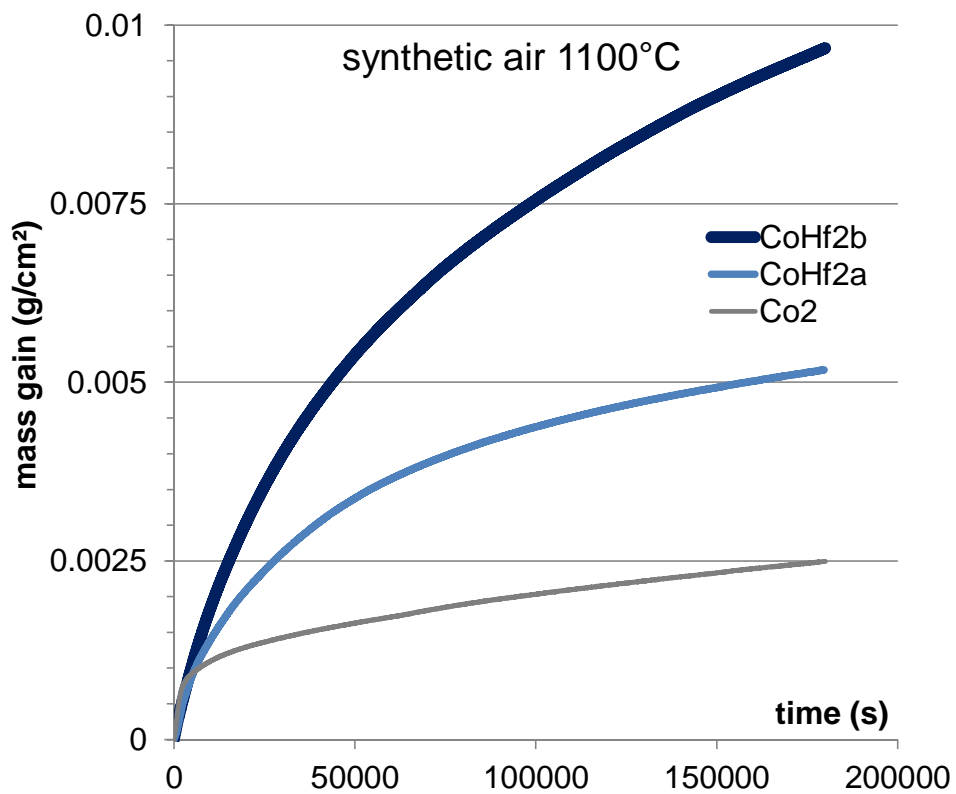
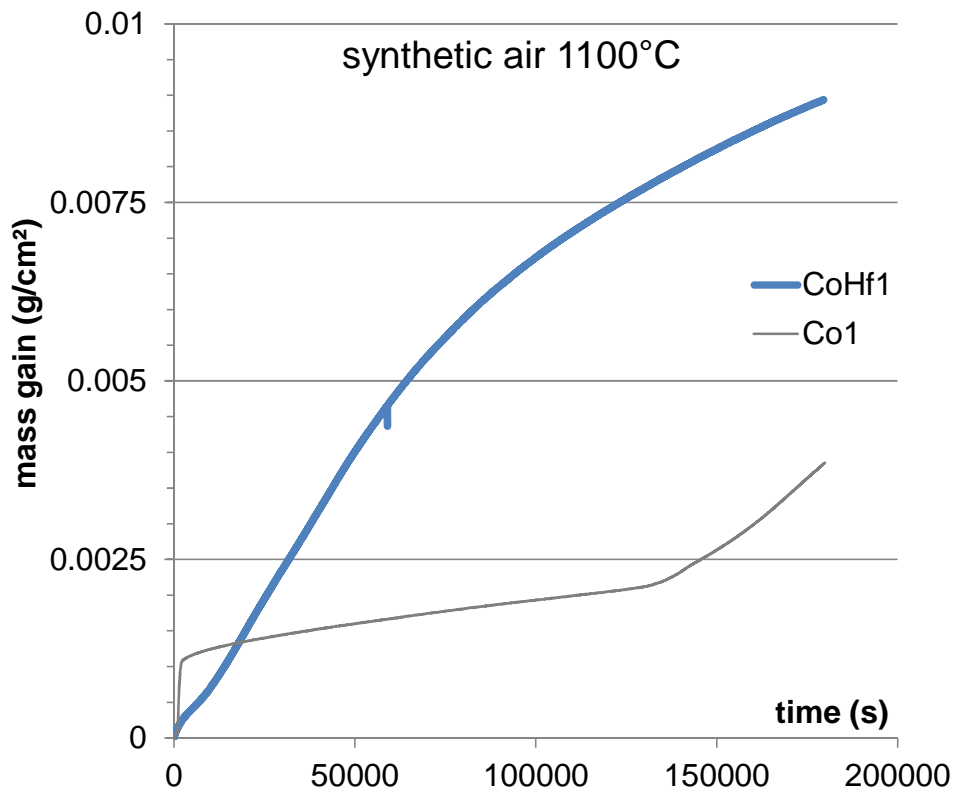


Fig. 2. Mass gain curves recorded for the three Hf-rich alloys with comparison with the corresponding Hf-free ternary alloys (top: 0.25C-containing alloys, bottom: 0.50C-containing alloys)

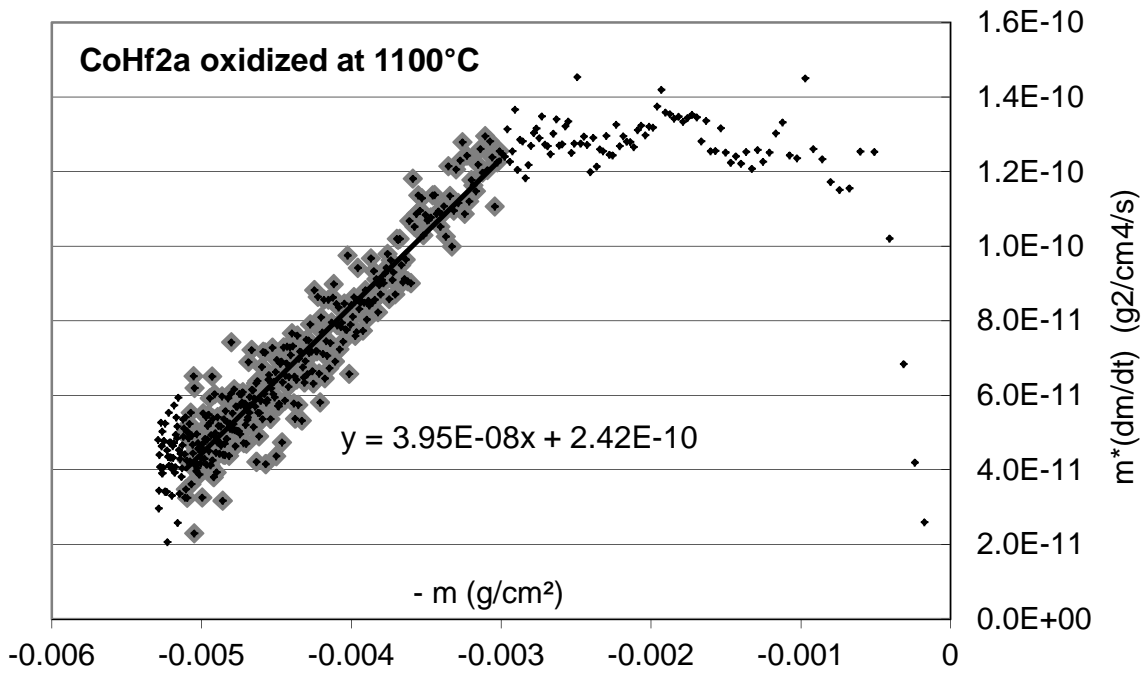


Fig. 3. Example of mass gain values plot according to the  $\{m \times dm/dt = f(-m) = K_p - m \times K_v\}$  to specify the isothermal kinetic constants  $K_p$  and  $K_v$  (here: the CoHf2a alloy)

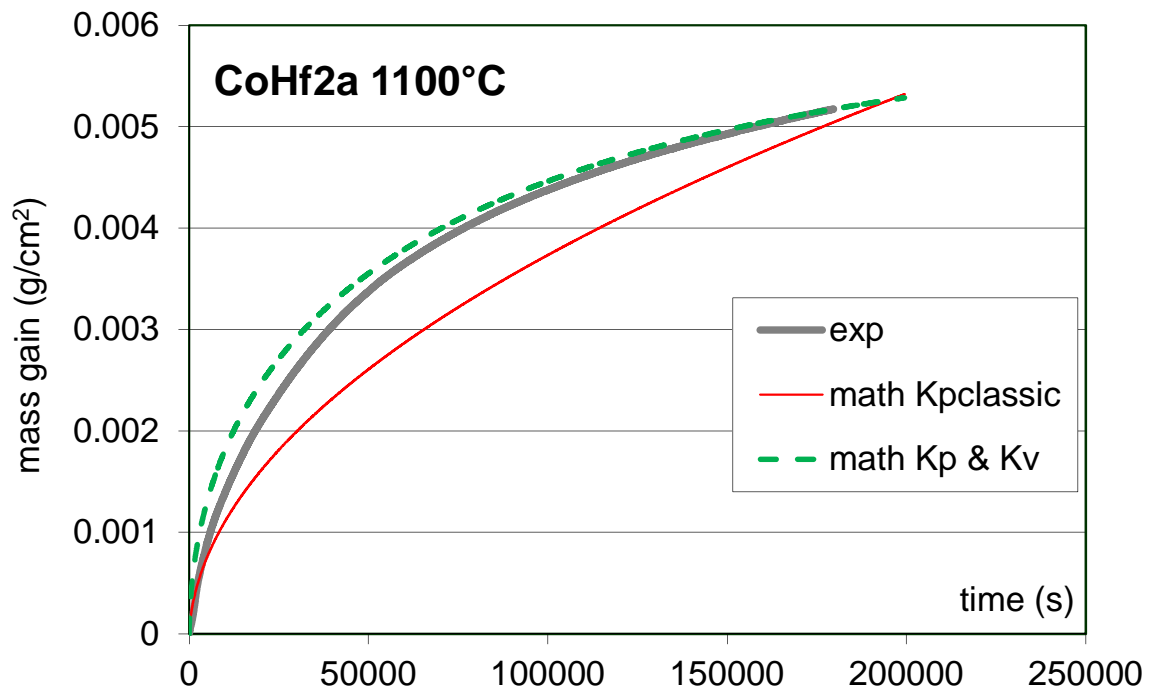


Fig. 4. Comparison, with the experimental mass gain curve (“exp”), of the mathematical curve drawn using the value of  $K_p$  only (issued from classical determination of parabolic constant, “math  $K_p$  classic”) and of the mathematical curve drawn using the values of  $K_p$  and  $K_v$  (issued from the treatment according to  $\{m \times dm/dt = f(-m) = K_p - m \times K_v\}$ , “math  $K_p$  &  $K_v$ ”); (here: the CoHf2a alloy)

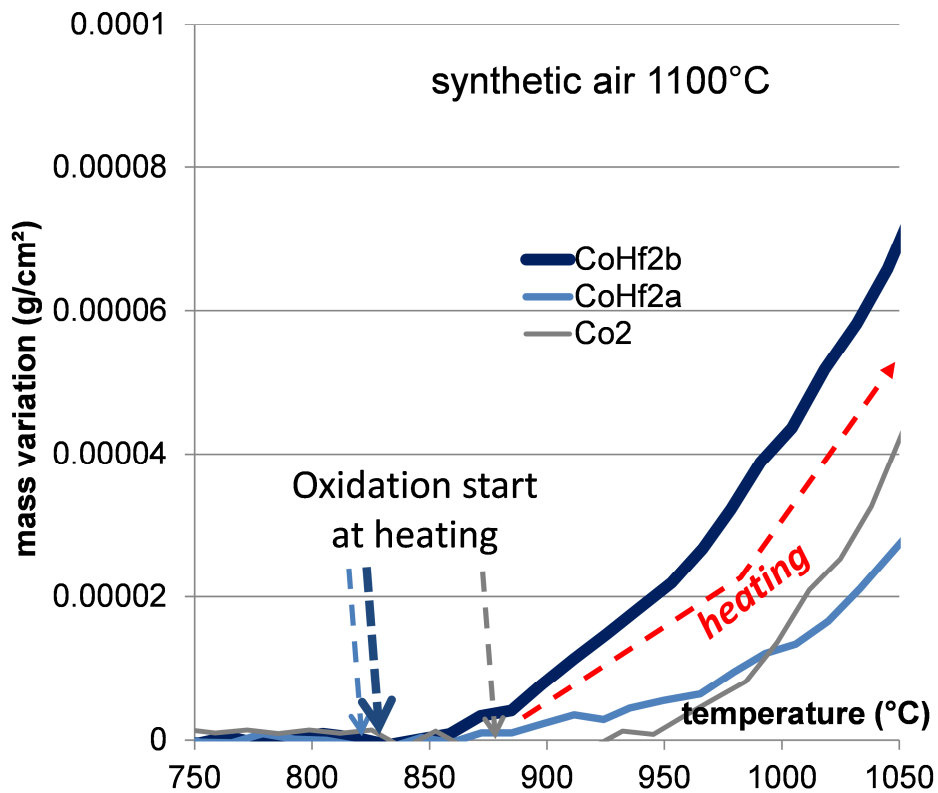
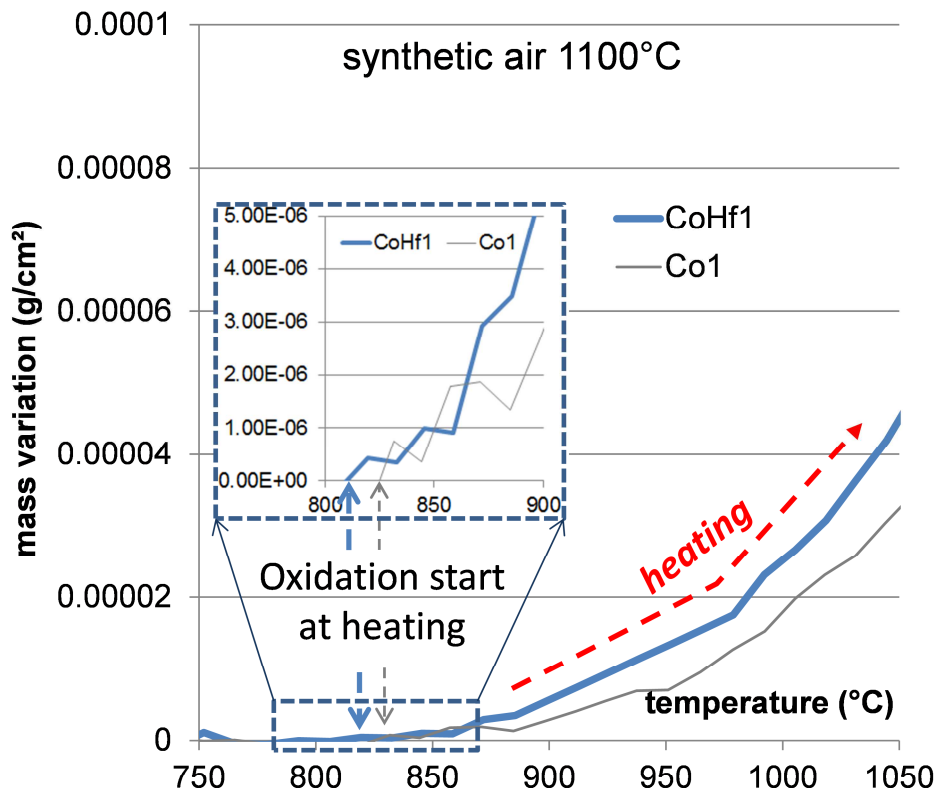


Fig. 5. Start of mass gain by oxidation during the heating (after correction of the thermogravimetry files from the air buoyancy variations);  
top: 0.25C-containing alloys (with inserted enlargement of the oxidation start part)  
bottom: 0.50C-containing alloys

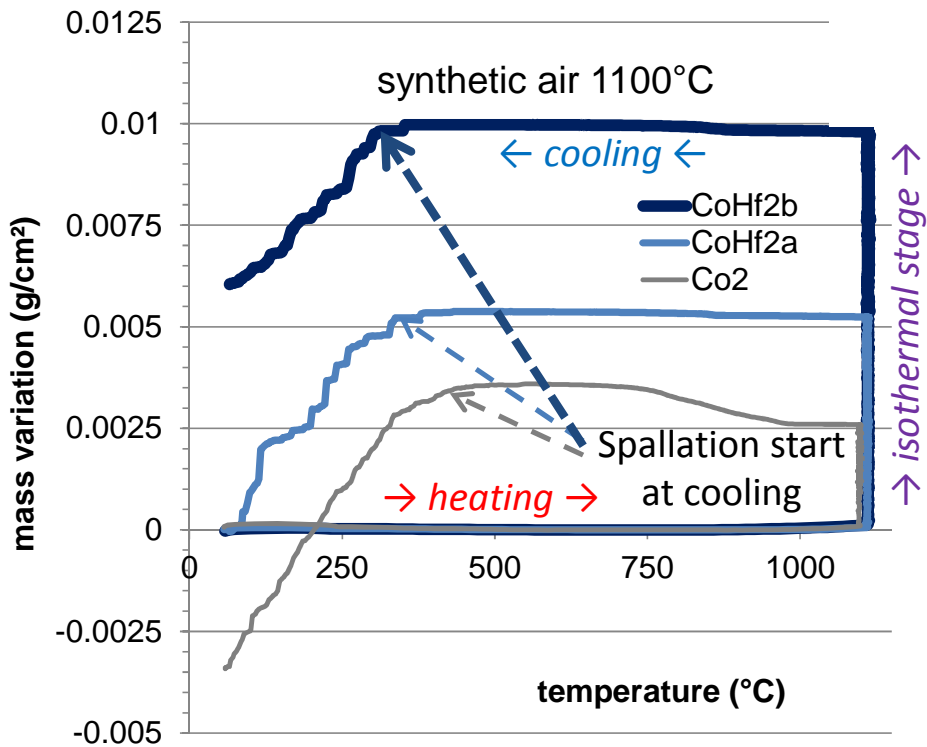
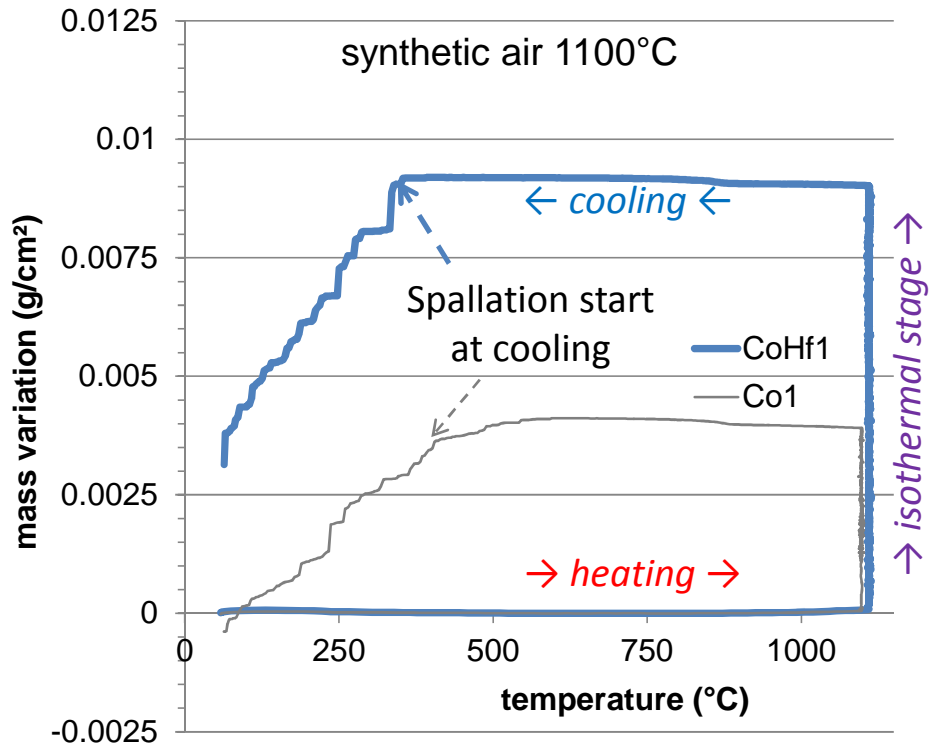


Fig. 6. Start of oxide scale spallation during the cooling (after correction of the thermogravimetry files from the air buoyancy variations); top: 0.25C-containing alloys, bottom: 0.50C-containing alloys

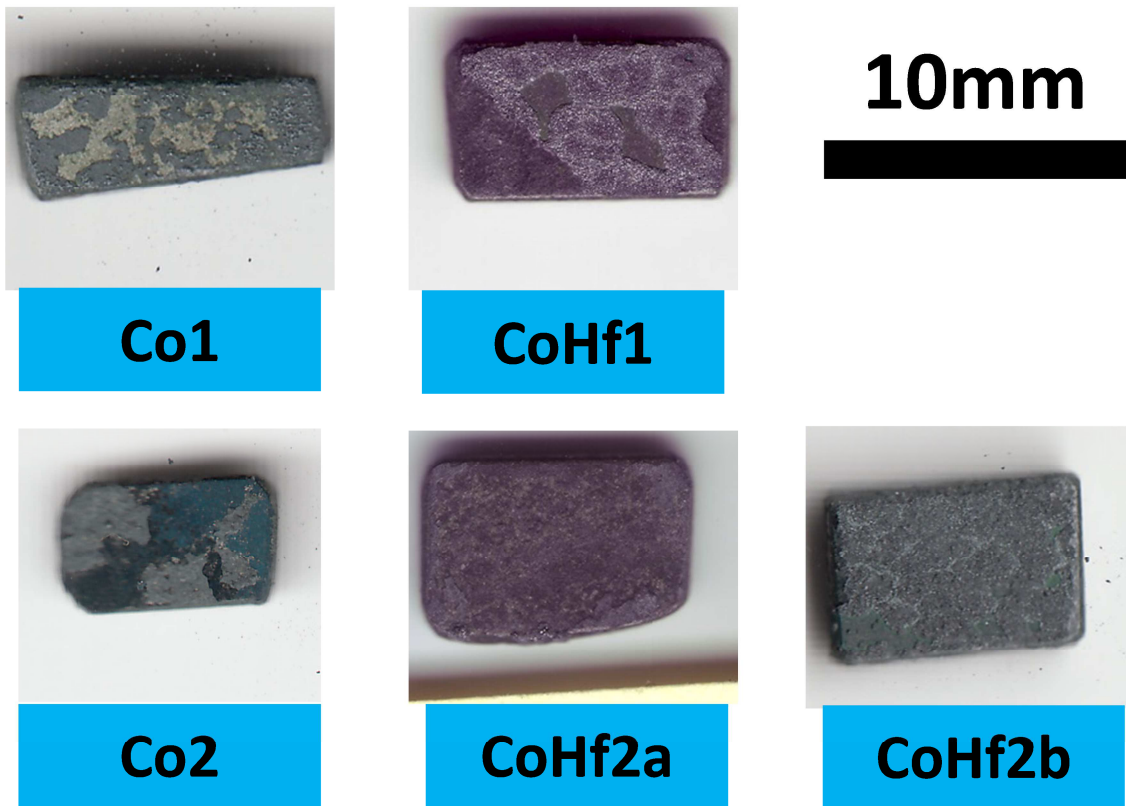


Fig. 7. Scanned views of one of the faces of the samples after oxidation test, for illustrating their oxidized states

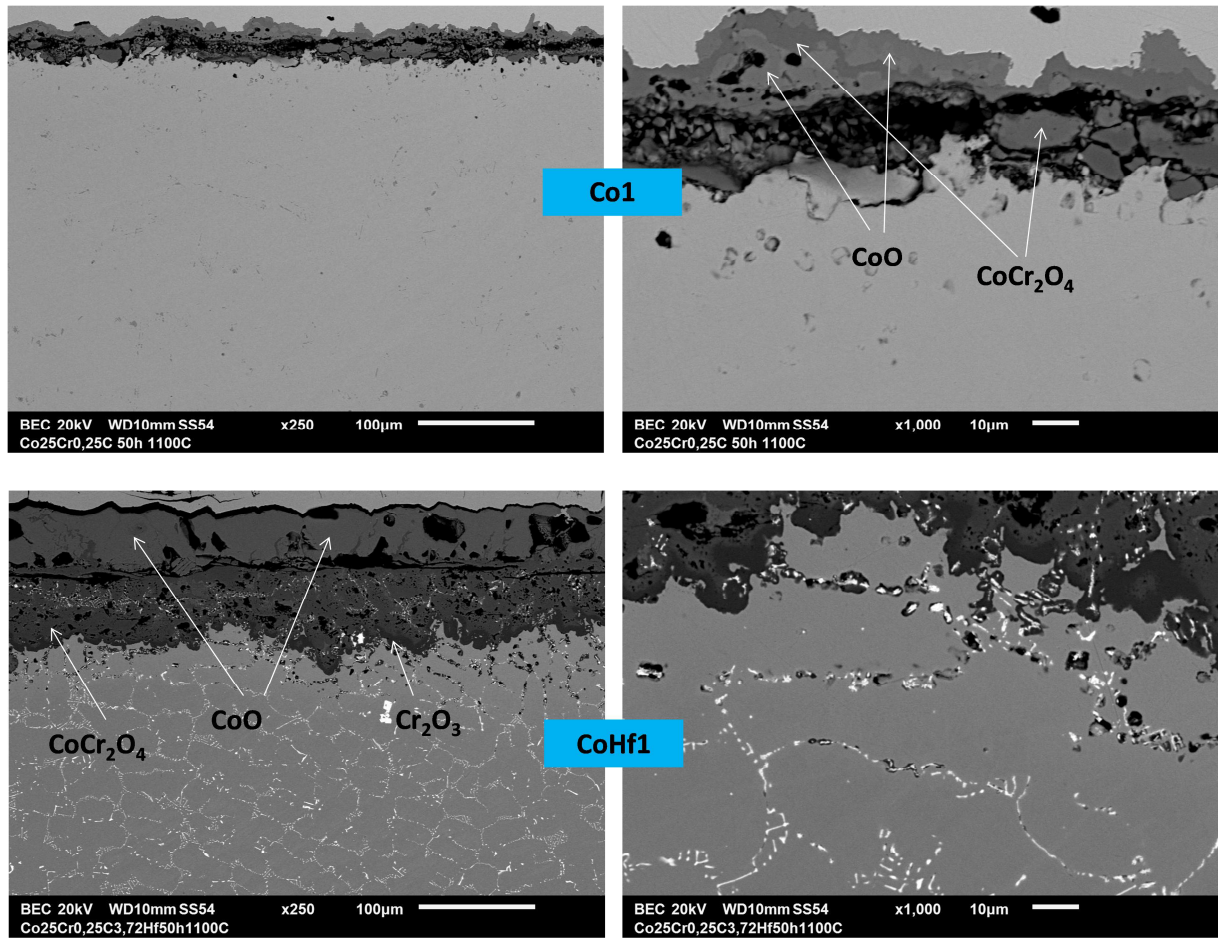


Fig. 8. Illustration of the surface states of the two 0.25C-containing alloys after oxidation test (cross sectional SEM/BSE examinations, SEM/EDS oxide determinations); top: the Hf-free Co1 alloy, bottom: the Hf-rich CoHf1 alloy

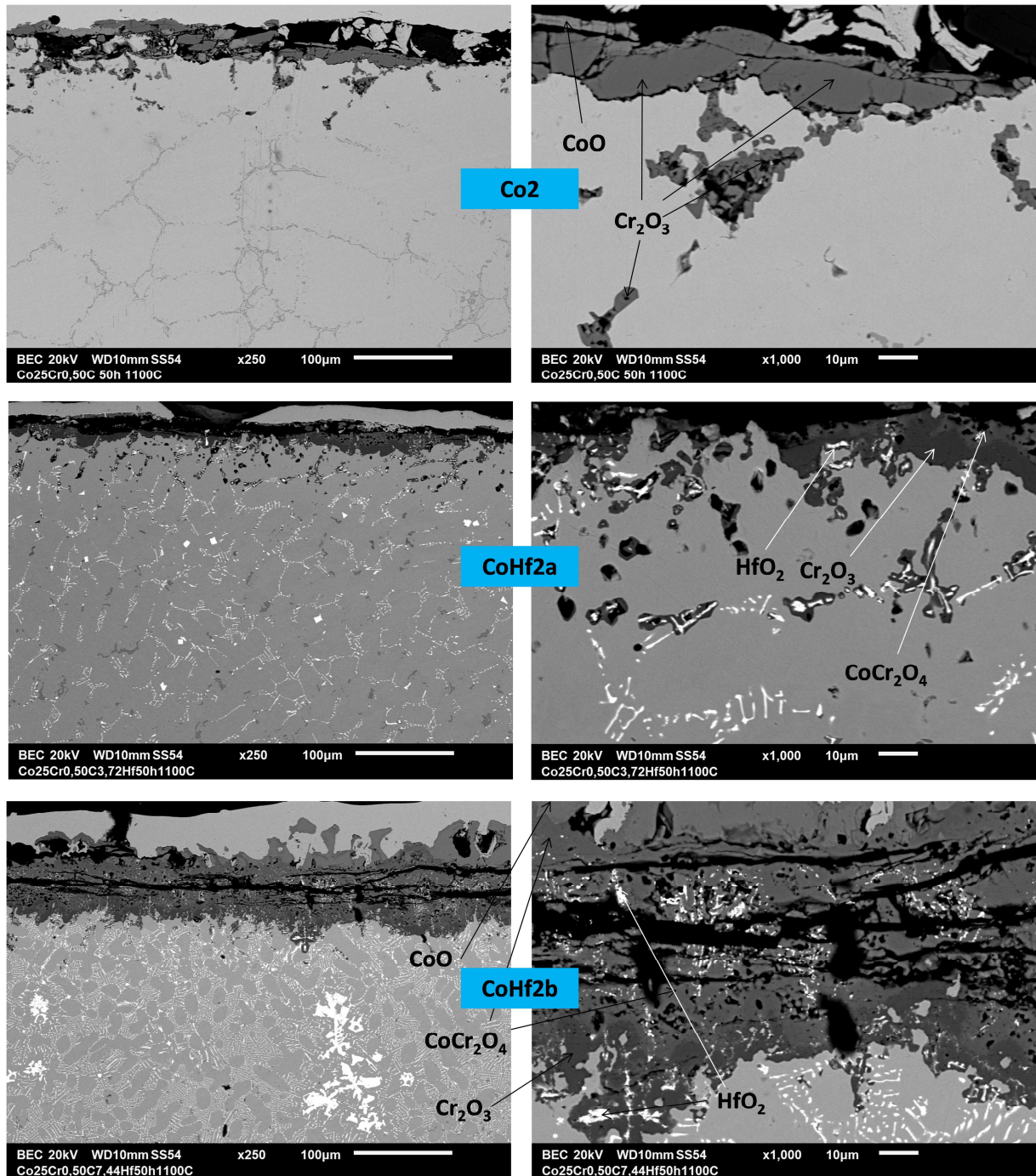


Fig. 9. Illustration of the surface states of the three 0.50C-containing alloys after oxidation test (cross sectional SEM/BSE examinations, SEM/EDS oxide determinations); top: the Hf-free Co<sub>2</sub> alloy, middle: the Hf-rich CoHf<sub>2a</sub> alloy, bottom: the Hf-rich CoHf<sub>2b</sub> alloy

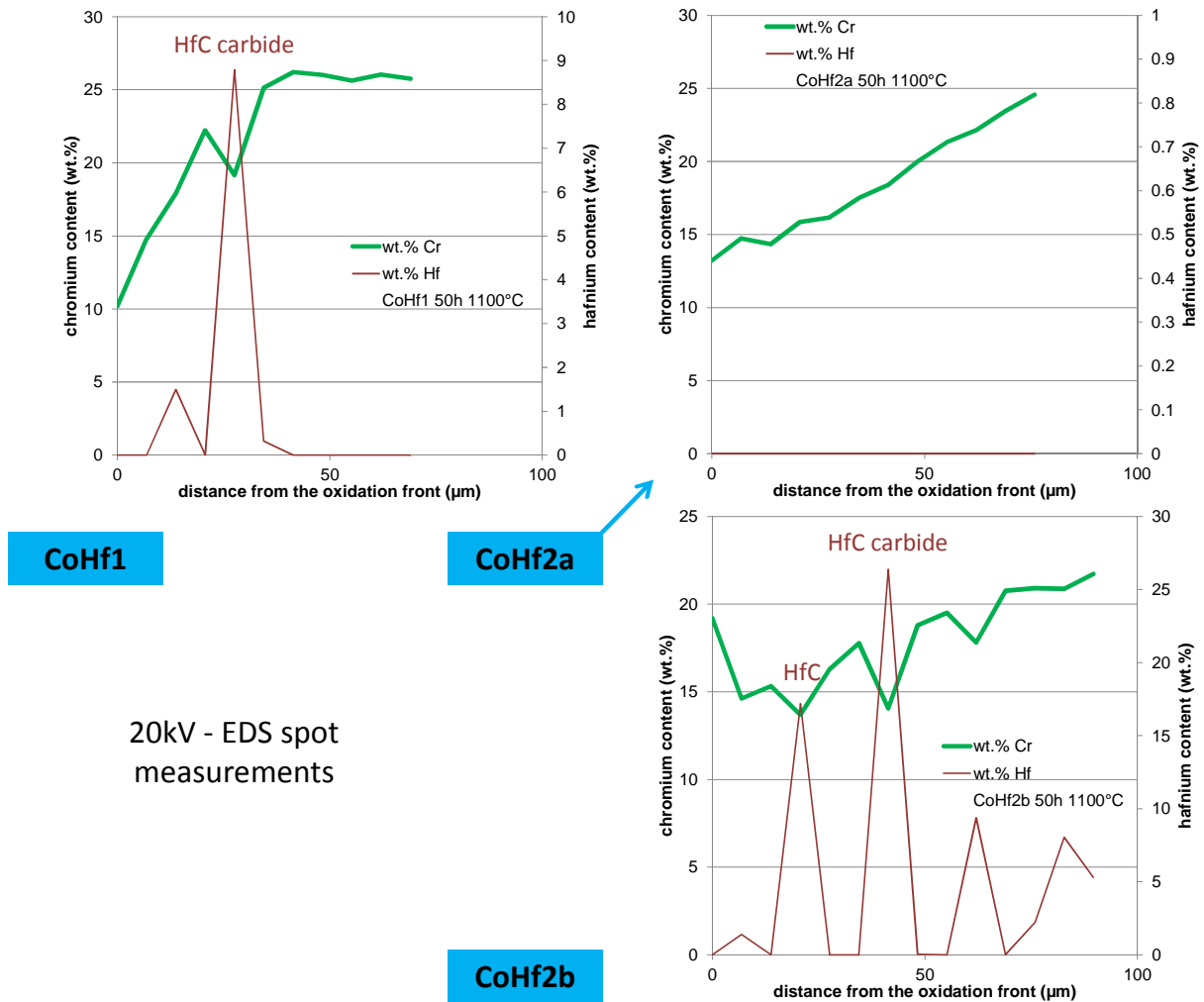


Fig. 10. Cr and Hf concentration profiles from the {oxide scale/alloy} interface (left side) toward the bulk (right side), perpendicularly to the sample surface (profiles plotted from EDS spot analyses performed perpendicularly to the {external oxide scale / alloy} interface on increasingly deep locations in the alloys)